Competing valence bond crystals in the kagome quantum dimer model

Didier Poilblanc[1] and Grégoire Misguich[2]

[1]*Laboratoire de Physique Théorique UMR-5152, CNRS and Université de Toulouse, F-31062 France*
[2]*Institut de Physique Théorique, CEA, IPhT, CNRS, URA 2306, F-91191 Gif-sur-Yvette, France*

The singlet dynamics, which plays a major role in the physics of the spin-1/2 quantum Heisenberg antiferromagnet (QHAF) on the kagome lattice, can be approximately described by projecting onto the nearest-neighbor valence bond (NNVB) singlet subspace. We revisit here the effective quantum dimer model, which originates from the latter NNVB-projected Heisenberg model via a nonperturbative Rokhsar-Kivelson-like scheme. By using Lanczos exact diagonalization on a 108-site cluster supplemented by a careful symmetry analysis, it is shown that a previously found 36-site valence bond crystal (VBC) in fact competes with a new type of 12-site "resonating-columnar" VBC. Interestingly, these two VBCs "emerge" in *different topological sectors*. The exceptionally large degeneracy of the ground-state multiplets (144 on our 108-site cluster) and the proximity of a $\mathbb{Z}_2$ dimer liquid have implications for the interpretation of numerical results on the QHAF, which are outlined. The possibility of a chiral VBC (i.e., spontaneously breaking time-reversal symmetry) is also discussed.

I. INTRODUCTION

The spin-1/2 quantum Heisenberg antiferromagnet (QHAF) on the kagome lattice (see Fig. 1) is the paradigm of frustrated quantum magnetism. Herbertsmithite[1] is an excellent experimental realization of such a kagome QHAF: Copper atoms carrying spin-1/2 degrees of freedom interacting antiferromagnetically are located on the sites of perfect kagome layers. In addition, deviations from an exact QHAF model like interlayer couplings, Dzyaloshinski-Moriya magnetic interactions,[2] intrinsic impurities,[3] etc., remain weak. The *absence* of any magnetic ordering at the lowest attainable temperatures[4] is the hallmark of a nonmagnetically ordered ground state as it may be realized in the ideal QHAF theoretical model (see below). However, it is still difficult to say whether the absence of a spin gap as inferred from the low-temperature behavior of the susceptibility[5] can also be interpreted as a generic feature of the perfect (theoretical) QHAF or whether it is due to an extrinsic perturbation, as one of those mentioned above.

On the theoretical side, the proliferation of many low-energy singlets revealed in early Lanczos exact diagonalizations (LEDs) of small clusters[6] strongly suggests that a nonmagnetically ordered phase could be stable in the kagome QHAF. Spin liquids (SLs) preserving all symmetries, both spin SU(2) and lattice translation, are the most fascinating and challenging candidates. Algebraic SLs,[7] or gapped SLs,[8,9] could be realized. Recently, density-matrix renormalization-group (DMRG) results[10] on large kagome strips found strong signals of a $\mathbb{Z}_2$ gapped SL. However, in variational Monte Carlo (VMC) studies[11] Z_2 SLs (whose fermionic formulations were recently proposed[12]) were found to have slightly higher energy than the algebraic SLs.

Valence bond crystals (VBCs) are other exotic candidates which, in contrast to SLs, spontaneously break the elementary (three-site) unit-cell translation symmetry, hence realizing a spontaneous (small) modulation characterized by a larger unit cell (named here "supercell"). VBCs with 12-site,[13] 18-site,[14] 6-site,[15] and 36-site[14,16,17] supercells have all been proposed in the literature as possible ground states (GSs) of the kagome

QHAF. Very schematically, a VBC is often drawn as a frozen hard-core covering of the lattice by nearest-neighbor spin singlets, so-called nearest-neighbor valence bonds (NNVBs). In reality, strong quantum fluctuations are expected to severely reduce the dimer order parameter. As shown in Fig. 1(a), the 36-site VBC shows an hexagonal lattice of resonating hexagons. It corresponds to a rather large $2\sqrt{3} \times 2\sqrt{3}$ supercell. The six-site VBC exhibits a 2×1 supercell with columnar dimer order as shown in Fig. 1(b). Both VBCs are of particular interest in this study and we shall refer to them as columnar VBCs (CVBCs) and hexagonal VBCs (HVBCs). In VMC studies, a (fermionic) HVBC can be stabilized by a very small next-NN *ferromagnetic* exchange coupling.[18] The observation of "diamond" patterns characteristic of the diamond VBC (DVBC) displayed in Fig. 2(b) [deriving from the "parent" VBC_0 of Fig. 2(a)] was observed in recent DMRG[10] studies. Also, closely related to VBC_0, the 12-site VBC of Ref. 13 shown in Fig. 2(c) displays a triangular lattice of resonating "stars" and shall be denominated as star VBCs (SVBCs).

II. GENERALIZED QUANTUM DIMER MODEL

All these theoretical studies show that singlet dynamics plays a major role in the low-energy physics of the spin-1/2 kagome QHAF. One possible route is therefore to approximate the QHAF by projecting onto the NNVB singlet *nonorthogonal* subspace.[19] Starting from the NNVB-projected Heisenberg model, an effective quantum dimer model (QDM) can be constructed via a nonperturbative Rokhsar-Kivelson (RK) -like scheme.[20] This procedure bears the enormous advantage to provide a mapping to an *orthogonal* hard-core dimer basis. Details can be, e.g., found in Refs. 21 and 22. Note that, although this method is certainly biased toward nonmagnetic (quantum disordered) states since it starts from the projection of the Heisenberg model onto the SU(2) *short-range* VB basis (to some extent, this approximation is supported by the earlier ED work on the kagome quantum AF[19]), generalized QDMs are potentially able to stabilize *equally well* VBCs and (gapped) dimer liquids ground states. In particular, it is known that simple QDMs can have robust (topological) $\mathbb{Z}_2$ dimer
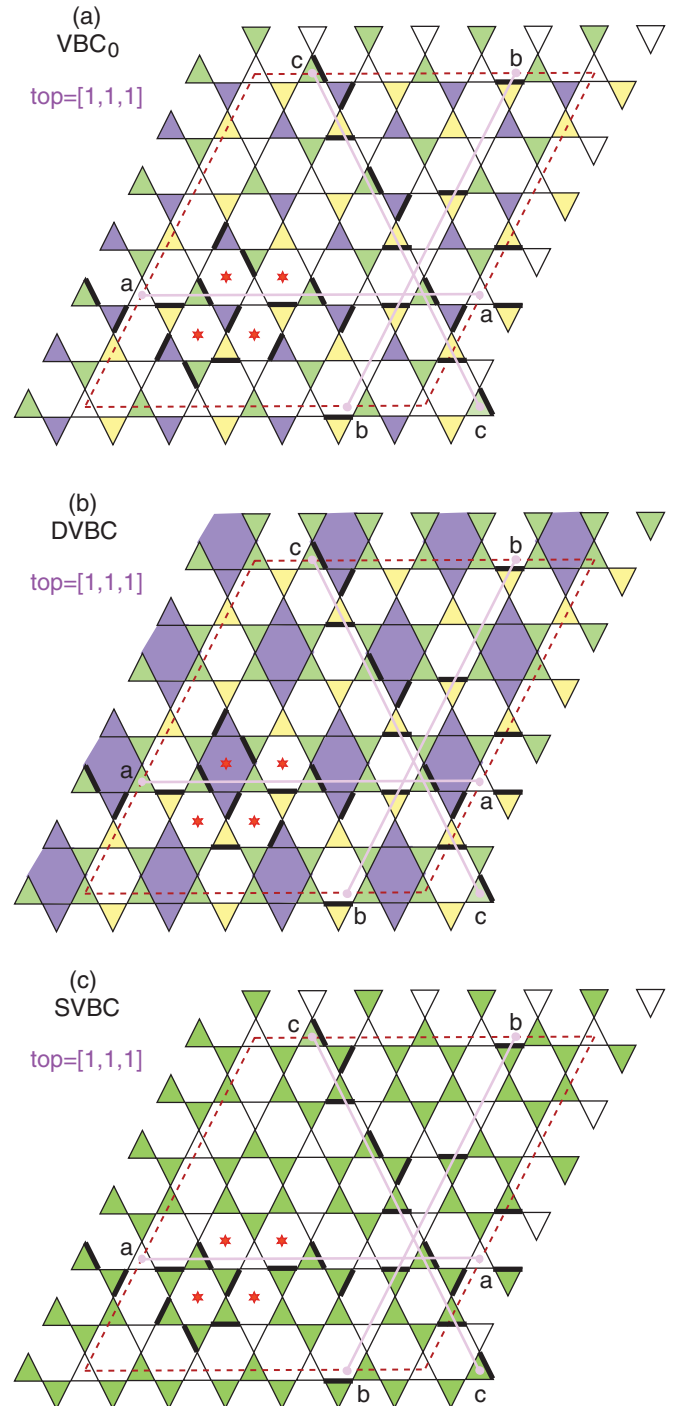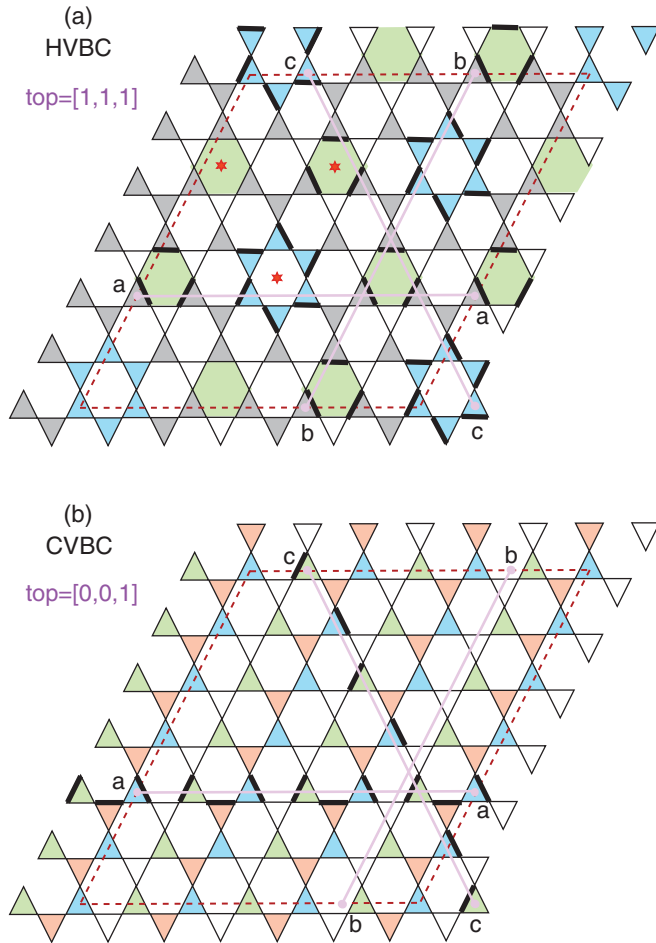
FIG. 1. (Color online) Kagome lattices. The 108-site clusters delimited by the (red) dashed lines are made of 6×6 unit cells of three-site up triangles. Periodic boundaries are used. The four topological sectors are determined by the parities of the number of dimers (black thick bonds) cut by the three a-a, b-b, and c-c closed loops along the three lattice directions shown (see text). For clarity, the hard-core dimers are only shown along the three cuts. "Defect" triangles with no dimers are left empty. (a) $2\sqrt{3} \times 2\sqrt{3}$ (36-site) HVBC showing resonating hexagons (shaded in green) and stars (shaded in blue) in the [1,1,1] topological sector. (b) 2×1 (six-site) CVBC with two types of up and two types of down triangles (all colored differently) in the [0, 0, 1] topological sector. The red stars indicate the inversion (π-rotation) centers.

liquid phases (the hard-core dimer equivalent of the gapped SL).[23,24]

Due to the orthogonal nature of the dimer basis, the kagome effective QDM can be diagonalized (by the Lanczos algorithm) on clusters up to 108 sites (6×6 three-site unit cells) providing clear signatures of the HVBC and the proximity (in some parameter space) of a quantum transition to a $\mathbb{Z}_2$ dimer liquid.[25] Note that, strictly speaking, in the QDM framework the spinon (i.e., the elementary $S = 1/2$ magnetic excitation) gap is pushed to infinity although some attempts have been carried out to bring spinons back into the picture.[26]

A remarkable and useful feature of the effective QDM is that it provides simple and direct access to topological properties of the ground state, which is more involved in SU(2) models.

FIG. 2. (Color online) VBC with 2×2 supercells in the [1,1,1] topological sector of the periodic $N = 108$-site cluster. (a) VBC_0 with four types of up (and down) triangles displayed with different colors except the defect triangles left empty (degeneracy $g = 8$). (b) The resonances of DVBC (colored diamonds) restore reflection symmetry with respect to the vertical and horizontal directions but suppress the $\pi/3$-rotation symmetry ($g = 12$). (c) SVBC has *higher symmetry* than VBC_0, resonating stars restoring reflection symmetry with respect to the crystallographic axes ($g = 4$).

On a periodic torus the parity of the numbers of dimers cut by two closed lines going along two orthogonal directions across the torus is conserved by the QDM Hamiltonian, hence defining four independent topological sectors. As clearly seen

in the "toy" RK QDM defined in Ref. 23, the $\mathbb{Z}_2$ dimer liquid is characterized by *topological symmetry breaking* with four degenerate GSs, one in each topological sector. The $\mathbb{Z}_2$ SL also carries (gapped) excitations, which are vortices of the dimer field (visons). In a cluster with an even (odd) number of sites, visons come in pairs[25] (in odd numbers[27]). Interestingly, a class of dimer liquid-VBC quantum phase transition can be described by a specific field theory[28] and has been observed

numerically by interpolating the Hamiltonian between the toy RK QDM and the effective kagome QDM.[25]

In the present work, we shall use topological symmetry extensively to revisit the effective QDM. From this refined analysis, we find that the previously identified 36-site HVBC competes with the new VBC.

We start here with the effective QDM derived in Ref. 22 [see Eq. (42) of this paper],

$$H_{\text{eff}}/J = -\frac{4}{5}\,\boxed{\diamond} + \frac{1}{5}\,\boxed{\diamond} + \frac{16}{63}\left(\boxed{\triangleright} + \boxed{\triangle} + \boxed{\square}\right) + \frac{2}{63}\left(\boxed{\triangleright} + \boxed{\triangle} + \boxed{\square}\right)$$
$$- \frac{16}{255}\left(\boxed{\triangleright} + \boxed{\triangle} + \boxed{\triangleright}\right) + \frac{1}{255}\left(\boxed{\star} + \boxed{\star} + \boxed{\star}\right) + 0\left(\boxed{\star} + \boxed{\star}\right) \tag{1}$$

The open diagrams correspond to kinetic processes around closed loops of length 6 (hexagons), 8, 10, or 12 (stars). In such a diagram, an alternating covering of (hard-core) dimers on the loop (i.e., a dimer on every second bond) is moved collectively by one step along the loop (i.e., it is "flipped"). Each diagram includes of course the reverse flipping action. Also, by definition, each diagram is meant for all (nonequal) loops of the lattices with the same topology, i.e., obtained under all possible translations, reflections, and rotations (i.e., under all elements of the space group of the lattice). The second kind of diagrams (colored ones) are diagonal terms that simply "count" the number of "flippable" loops of the first kind. More details can be found, e.g., in Refs. 21 and 22. Note that, in contrast to Ref. 25, Eq. (1) includes infinite order resummation of all the processes (loops) restricted to a single hexagon. This, however, only leads to very small changes of the values of the coefficients of H_{eff} compared to Ref. 25. Note also that the stars have vanishing amplitudes at all orders.

III. TOPOLOGICAL PROPERTIES AND SYMMETRY ANALYSIS

The generalized QDM is investigated by Lanczos exact diagonalization of the finite 108-site cluster of the kagome lattice made of 6×6 unit cells of three-site up triangles and delimited by (red) dashed lines in Figs. 1 and 2. Periodic boundary conditions are used in the horizontal a-a and b-b (at $60°$) directions so that the system is topologically equivalent to a torus, providing global invariance under the translation group $\mathcal{T}$. On such a geometry, the generalized QDM Hamiltonian bears interesting topological properties: its Hilbert space of (orthogonal) NNVB hard-core coverings can be split in four disconnected topological sectors, which are conserved by the QDM Hamiltonian. To determine the topological sector of a given dimer configuration, one simply needs to count the number of dimers (black thick bonds) cut by the three a-a, b-b, and c-c closed loops along the three lattice directions shown in Figs. 1 and 2. We shall label these sectors as $[\alpha,\beta,\gamma]$ where α, β, and γ are 0 or 1 depending on whether the numbers of dimers cut by the corresponding loops are even or odd, respectively. Every cluster of $P \times P$ unit cells (with $N = 3P^2$ sites) contains a "symmetric" topological sector $[\alpha,\alpha,\alpha]$ with

$\alpha = 0$ or $\alpha = 1$ for $P = 4p$ or $P = 4p + 2$, respectively. Flipping the dimers along a closed loop that goes around the torus, e.g., along the a-a direction, switches the parity of the number of dimers cut in the two other directions, e.g., along b-b and c-c. For the 108-site cluster of interest here, one can then build the four topological sectors $T_0 = [1,1,1]$, $T_1 = [1,0,0]$, $T_2 = [0,1,0]$, and $T_3 = [0,0,1]$. All configurations of each topological sector can be obtained separately by constructing an initial dimer configuration belonging to the targeted sector and then by applying recursively loop-flipping operators of the type of Eq. (1) to generate (numerically) new configurations until the Hilbert space is complete.

In order to block-diagonalize the Hamiltonian matrix in each topological sector, one can make use of all space-group symmetries leaving each sector globally invariant. The corresponding point group $\mathcal{G}(T_\alpha)$ depends on the topological sector T_α. Note that we use here the center of the hexagon as the common origin for all point-group elements. The full point group $\mathcal{G} = C_{6v}$ of the infinite lattice can be used for the "fully symmetric" $T_0 = [1,1,1]$ topological sector. In contrast, the $2\pi/3$ rotation is lost in the $T_1 = [1,0,0]$, $T_2 = [0,1,0]$, and $T_3 = [0,0,1]$ topological sectors so that the invariant point group is reduced to $\mathcal{G} = C_{2v}$. Each of these three topological sectors and their two corresponding (orthogonal) reflection symmetry axes are related by $2\pi/3$ and $4\pi/3$ rotations.

In practice, one can specify a fixed momentum $\mathbf{K}$ in the Brillouin zones (BZs) of Fig. 3 and diagonalize the Hamiltonian separately in all irreducible representations (IRREPs) of its little group $\mathcal{G}_{\mathbf{K}}$ [which is defined by all the elements of $\mathcal{G}(T_\alpha)$ leaving $\mathbf{K}$ invariant in the BZ]. All little groups are listed in Table I for the relevant $\mathbf{K}$ points of the $N = 108$ cluster. The size of the Hilbert space (i.e., the number of orthogonal states) can then be reduced from the full size $2^{N/3+1} \simeq 137 \times 10^9$ by (i) a factor 4 for each topological sector, (ii) a factor $N/3 = 36$ by using translation symmetry, and (iii) a factor card$\{\mathcal{G}_{\mathbf{K}}\}$ (see Table I) by using point symmetry. Hence after proper construction of the new "symmetrized" basis states in each IRREP, the linear sizes of the corresponding Hamiltonian "blocks" range from $\sim 80 \times 10^6$ ($\mathcal{G}_{\mathbf{K}} = C_{6v}$) to $\sim 960 \times 10^6$ ($\mathcal{G}_{\mathbf{K}} = Id$). In the following, each IRREP will be labeled by its momentum/topological sector according to Fig. 3 (different combination of letters, subscripts, and superscripts are used to
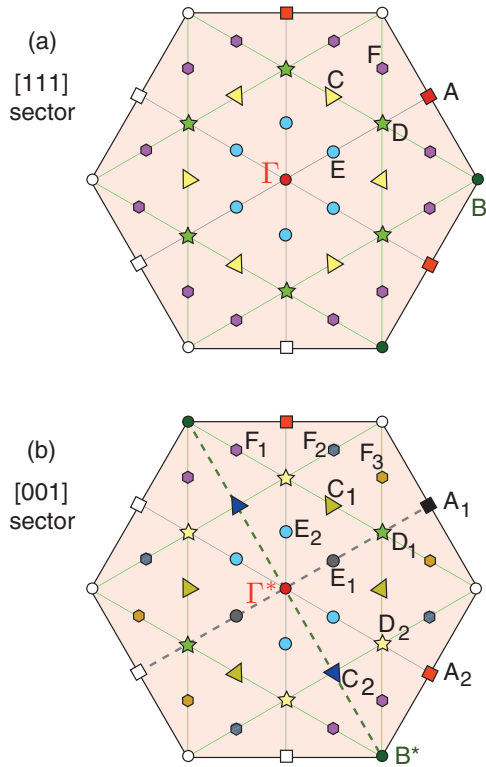
FIG. 3. (Color online) 36 available momenta of the 108-site cluster (6×6 up triangles) in the first Brillouin zone. Topological sectors have to be distinguished (as done on graph) because of their different point groups (see text). *Equivalent* momenta are represented by the same (filled) symbols. Translation by a reciprocal-lattice vector (thin lines) of the momenta at the border of the first BZ are shown by open symbols (correspond to the *same* momenta). The dashed lines in (b) represent the two (orthogonal) reflection symmetry axes of the C_{2v} group.

distinguish all of them) and by the characters (r_3, r_2, σ), which refer to $2\pi/3$ rotations, parity under inversion, and reflection about the momentum direction, respectively, whenever such symmetries are relevant (which depends on $\mathcal{G}_\mathbf{K}$). For the center of the BZ Γ, σ refers to the reflection along one of the lattice directions (consistently with Ref. 29) while, for the center Γ^*, it refers to the reflection along the axis perpendicular to the c direction (i.e., along the momentum A_1 in reciprocal space).

IV. SPONTANEOUS SYMMETRY BREAKING AND DEGENERACIES OF VBCs

The spectrum of a system that spontaneously breaks some lattice symmetries at zero temperature shows some ground-state degeneracies. Moreover, these degeneracies occur between levels belonging to different IRREPs of the lattice symmetry group. The simplest example is that of a $\mathbb{Z}_2$ symmetry breaking, where a state that in the "even" (topological) sector is degenerate with a state in the "odd" sector. In a finite-size system these degeneracies are only approximate, but they are expected to become exponentially precise when increasing the system size. In turn, the presence of degeneracies is almost always the indication of some spontaneous symmetry breaking, and this type of signature

TABLE I. Little groups $\mathcal{G}_\mathbf{K}$ for all $\mathbf{K}$ momenta of Figs. 3(a) and 3(b) corresponding to the $T_0 = [1, 1, 1]$ and $T_3 = [0, 0, 1]$ topological sectors, respectively.

$\mathbf{K}$	$\mathcal{G}_\mathbf{K}$	Card$\{\mathcal{G}_\mathbf{K}\}$	$\mathbf{K}$	$\mathcal{G}_\mathbf{K}$	Card$\{\mathcal{G}_\mathbf{K}\}$
Γ	C_{6v}	12	B^*	C_v	2
A	C_{2v}	4	C_1	Id	1
B	C_{3v}	6	C_2	C_v	2
C	C_v	2	D_1	C_v	2
D	C_v	2	D_2	Id	1
E	C_v	2	E_1	C_v	2
F	Id	1	E_2	Id	1
Γ^*	C_{2v}	4	F_1	Id	1
A_1	C_{2v}	4	F_2	Id	1
A_2	C_I	2	F_3	Id	1

has been widely used in exact-diagonalization studies to detect ordered phases.[29]

If one knows the VBC pattern/symmetry, it is relatively easy to compute the IRREP that should appear in the ground-state multiplet. Let us denote by $|1\rangle, \ldots |d\rangle$ the states obtained by putting the VBC pattern on the lattice in all the possible positions/orientations. For a sufficiently large lattice they can be considered as orthogonal to each other, and they transform into each other under the action of the lattice symmetry group $G = \mathcal{G} \otimes \mathcal{T}$: for any symmetry $g \in G$ and for any state $|i\rangle$, there exists another state $j = f(g, i)$ such that $g|i\rangle = |j\rangle$. We assume in particular that the latter equation holds without any phase factor. Such a ground-state multiplet defines nothing but a (reducible) *representation* of dimension d of the group G. Determining the associated ground-state quantum numbers amounts to decomposing this representation over the IRREPs of G, which is a standard task in group theory. If we denote by ρ some IRREP of G, the number n_ρ of ground states that should appear in the symmetry sector ρ is given by a character formula:

$$n_\rho = \frac{1}{|G|} \sum_{g \in G} \chi_\rho(g^{-1}) \text{Tr}_{|1\rangle, \ldots |d\rangle}(g), \qquad (2)$$

where $\chi_\rho(g^{-1})$ is the character of ρ on the group element g^{-1}, $|G|$ is the total number of symmetries, and $\text{Tr}_{|1\rangle, \ldots |d\rangle}(g)$ is the number of VBC states that are invariant under g: $g|i\rangle = |i\rangle$. The latter quantity only depends on the symmetries of the VBC and not on the full wave function. It can therefore be computed using "simplified" states with the correct symmetries. It can sometimes be reduced to a *single* (nonresonant) covering, or a linear combination of 2^{n_cell} coverings for resonating states with n_cell supercells ($n_\text{cell} = N/\mathcal{N}$). In any case, from the group characters χ_ρ and the symmetries of the VBC, the multiplicities n_ρ can be systematically computed and compared to the spectrum obtained in LEDs.

We have computed these multiplicities for a few VBCs with a 2×2 or 2×1 supercell on the 108-site cluster. These multiplicities were obtained in a fixed topological sector, in order to compare to the LED results (next section). To do so, the lattice symmetry group was simply restricted to the elements that conserve the topological sector, i.e., excluding $2\pi/3$ rotations in the $[0, 0, 1]$, $[0, 1, 0]$, and $[1, 0, 0]$ sectors. The results are shown in Table II. The VBCs named CVBC is the simplest,

TABLE II. Quantum numbers of the GS multiplet for VBC with $m \times n$ supercells of $\mathcal{N} = 3mn$ sites. The letters refer to the momenta of Fig. 3 (with their multiplicities in brackets) in the two topological sectors [1,1,1] and [0, 0,1]. The character related to $2\pi/3$ rotations ($r_3 = 1, j, j^2$), parity under inversion ($r_2 = +,-$), and reflection about the momentum direction ($\sigma = +,-$) are denoted as (r_3, r_2, σ). "$\pm$" means that *both* even and odd GS are present and "$\times$" stands for "symmetry not relevant" (e.g., $2\pi/3$ rotation and hence r_3 is irrelevant in the [0, 0,1] topological sector). VBC$_0$, DVBC, and SVBC are 8-fold, 12-fold, and 4-fold degenerate, respectively. CVBC, rVBC$_1$, rVBC$_1'$, and rVBC$_3$ have the same degeneracy $g = 8$ in the [0, 0,1] sector, i.e., $g = 8 \times 3 = 24$ including all three topological sectors while rVBC$_2$ has $g = 16 \times 3 = 48$. The last line corresponds to the $\mathbb{Z}_2$ dimer liquid ($g = 4$).

VBC	Cell	Γ ($\times 1$)	A ($\times 3$)	Γ^* ($\times 1$)	A_2 ($\times 2$)	A_1 ($\times 1$)
VBC$_0$	2×2	$(1, +, \pm)$	$(\times, +, \pm)$			
DVBC	2×2	$(1, +, +)$	$(\times, +, +)^a$			
		$(j, +, \times)^b$	$(\times, +, -)$			
SVBC	2×2	$(1, +, +)$	$(\times, +, +)$			
CVBC	2×1			$(\times, \pm, \pm)$	$(\times, \pm, \times)$	
rVBC$_2$	2×2			$(\times, \pm, \pm)$	$(\times, \pm, \times)^a$	$(\times, \pm, \pm)$
rVBC$_1$	2×2			$(\times, \pm, +)$	$(\times, \pm, \times)$	$(\times, \pm, +)$
rVBC$_1'$	2×2			$(\times, +, +)$	$(\times, \pm, \times)$	$(\times, +, +)$
				$(\times, -, -)$		$(\times, -, -)$
rVBC$_3$	2×2			$(\times, +, \pm)$	$(\times, +, \times)^a$	$(\times, +, \pm)$
VBC*	2×2			$(\times, +, \pm)$	$(\times, +, \times)^a$	$(\times, +, \pm)$
$\mathbb{Z}_2$	1×1	$(1, +, +)$		$(\times, +, +)$		

[a]Twofold degenerate GS with this quantum number.
[b]Twofold degenerate IRREP ($r_3 = j$ and j^2).

since, as far as the symmetries are concerned, it can be reduced to a single dimer covering. CVBC is displayed in Fig. 1(b), and has first been proposed in Ref. 15. It has a 2×1 supercell and a degeneracy equal to 8 (for each of the three topological sectors, so 24 in total). The VBC$_0$ of Fig. 2(a) can also be reduced to a single dimer covering but, in contrast to the CVBC, belongs to the [1.1,1] topological sector. Its degeneracy is 24. The other VBCs we considered involve some resonance between different dimer configurations. The rVBC$_2$ [see Fig. 4(a)] can be constructed from the CVBC configuration by applying some resonance operators σ^x (notation of Ref. 23) on a quarter of the hexagons [colored in blue in Fig. 4(a)], to shape a 2×2 supercell:

$$|r\text{VBC}_2\rangle = \prod_{h=1,\ldots,9} \left(1 + \alpha \sigma_h^x\right)|\text{CVBC}\rangle.$$

Doing so simultaneously enlarges the supercell and doubles the degeneracy (16). If the coefficient α is set to 1, one restores a reflection symmetry ($\sigma = +$) and we get another VBC, named $|r\text{VBC}_1\rangle$ and with degeneracy 8. By applying the resonance operators on the other hexagon sublattice [colored in orange in Fig. 4(b)], one obtains another resonating VBC, $|r\text{VBC}_1'\rangle$ shown in Fig. 4(b), with the same degeneracy (8) but different quantum numbers (the symmetry axis is now that of the wave vector B^*, i.e., along the c direction). Another resonating crystal, $|r\text{VBC}_3\rangle$ shown in Fig. 4(c), with no reflection symmetry (in contrast to the previous ones) but with inversion symmetry with respect to the centers of all the hexagons, can also be constructed in the [0, 0,1] topological sector but using longer range dimers. We believe there is a similar VBC (that we name VBC*) that bears exactly the same symmetry property and which could be represented solely in terms of (hard-core) NN dimers, probably requiring a more involved resonance structure. Finally, the SVBC discussed in Ref. 13 is made of resonating "stars" (12-dimer loops) and

also has a 2×2 supercell. Similarly, the DVBC is made of resonating diamonds (eight-dimer loops). But unlike the previous examples, these two crystals belong to the [1,1,1] sector.

It appears that the trivial IRREP [$\Gamma(+, +, +)$ or $\Gamma^*(\times, +, +)$] appears *exactly once* in all the VBCs we have listed so far. This is in fact a general property of such kind of broken symmetry phase. Indeed, the multiplicity of Γ is just a special case of Eq. (2) where the character χ_Γ is constant and equal to unity. We thus have

$$n_\Gamma = \frac{1}{|G|} \sum_{g \in G} \text{Tr}_{|1\rangle,\ldots|d\rangle}(g).$$

However, $\text{Tr}_{|1\rangle,\ldots|d\rangle}(g)$ is nothing but the number of states that are invariant under the symmetry g. So n_Γ can be written using the stabilizers Stab(i) or each state $|i\rangle$:

$$n_\Gamma = \frac{1}{|G|} \sum_{i=1}^{d} |\text{Stab}(i)|.$$

But since all the stabilizers have the same number of elements, $|\text{Stab}(i)| = |G|/d$, we just find $n_\Gamma = 1$. In Sec. VI this remark will allow us to show that a particular multiplet of low-lying states cannot be interpreted as a single conventional VBC.

V. NUMERICAL RESULTS

We have used the Lanczos exact-diagonalization technique to obtain the low-energy spectra of the QDM Hamiltonian in each IRREP. Computations have been performed on the Altix SGI cluster at CALMIP (Toulouse), in particular on the Altix UV node providing 96 CPUs allocating 1024 Gb of fast access RAM. Typically, only 200 Lanczos iterations were sufficient to get at least five or six of the lowest eigenenergies (in each IRREP) with full machine (double) precision.[30]
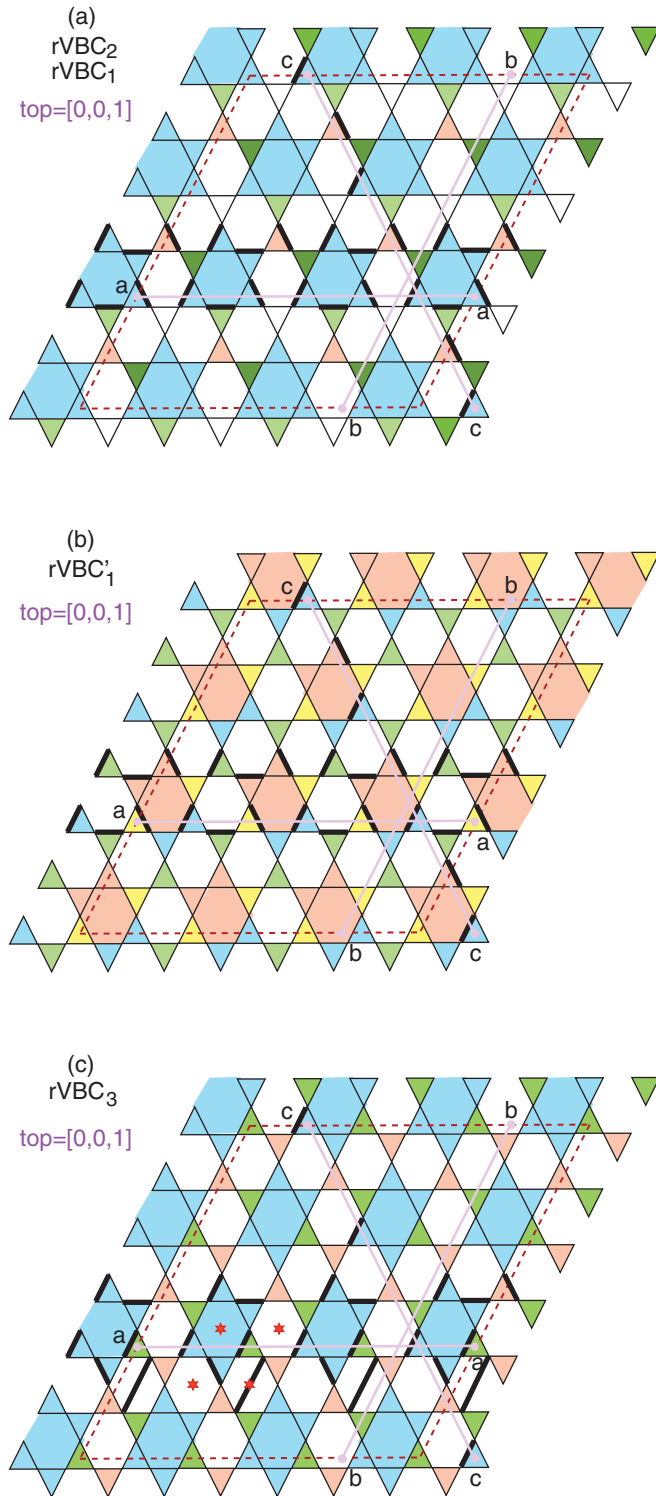
FIG. 4. (Color online) Resonant VBC with 2×2 supercells in the $[0, 0, 1]$ topological sector of the periodic $N = 108$-site cluster. Resonating ten-dimer (a),(c) and eight-dimer (b) loops (see text) are represented by shaded areas. (a) When $\alpha = 1$ (see text) a symmetry axis perpendicular to the c direction is restored (light and dark green triangles become equivalent). (b) The pattern exhibits a reflection symmetry with respect to the c direction. (c) Inversion symmetry with respect to the centers of all the hexagons is present. Dimers beyond NNs have been used.
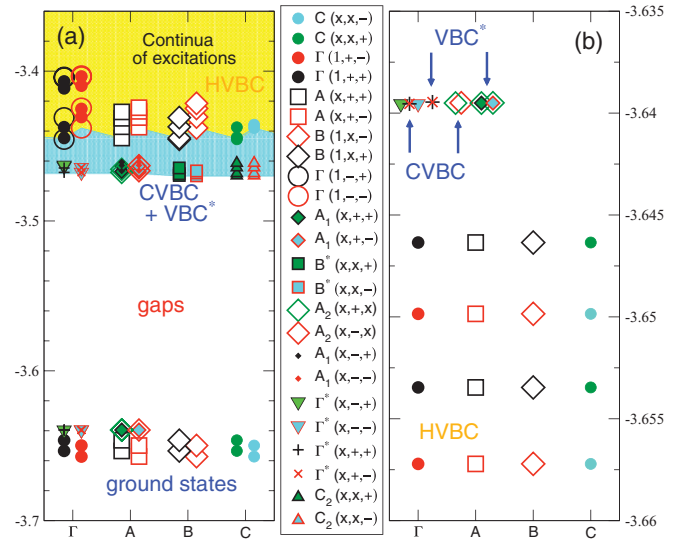

FIG. 5. (Color online) (a) Low-energy spectrum of the 108-site cluster in the $T_0 = [1,1,1]$ and $T_3 = [0,0,1]$ (degenerate with $[0,1,0]$ and $[1,0,0]$) topological sectors. Different symbols distinguish different momenta and topological sectors [see Figs. 3(a) and 3(b)] and IRREPs labeled as "(r_3, r_2, σ)" (see text). Only a few levels corresponding to the onsets of the two continua (shaded areas) are shown. (b) Zoom in of the (quasi)ground states. An Ising degeneracy (see text) is reflected by the (almost) perfect equal spacings between the HVBC ground states.

Figure 5(a) shows the obtained low-energy spectra at the most relevant momenta and in the two topological sectors $[1,1,1]$ and $[0, 0,1]$. For each of these sectors, we can see a group of quasidegenerate levels named "ground-state manifold" and a dense accumulation of levels at higher energy. This clearly reflects the presence of two continua of excited states above two (slightly different) thresholds separated from the GS manifolds by two gaps. Note that the energy spectra at the other momenta (D, E, and F in Fig. 3) are not shown on this picture since they only contain excited states beyond the gaps and no level belonging to the ground-state manifold. Figure 5(b) shows a zoom in of the ground-state manifold, which reveals two subgroups corresponding to each topological sector.

In agreement with Ref. 25, the quantum numbers of the GS levels in the "symmetric" $[1,1,1]$ topological sector correspond exactly to those predicted (see Ref. 29 for details) for the 36-site HCVB schematically shown in Fig. 1. In addition, we find here some very remarkable (Ising-like) fine structure with equally spaced subsubgroups of levels, which shall be discussed later on. The numerical values of these eigenenergies reported in Table III reveal almost exact degeneracies within less than 10^{-5} (in units of the exchange constant J).

The investigation of the $[0, 0,1]$ and the two other equivalent topological sectors was overlooked in Ref. 25. Interestingly, Fig. 5(b) reveals a new subgroup of energy levels within $\sim 6 \times 10^{-3} J$ from the $[1,1,1]$ GS subgroup. Their energies are listed in Table IV showing again almost perfect degeneracies within subsubgroups of levels. The quantum numbers of these states can be straightforwardly compared to the expected quantum numbers for the VBC shown in Table II. Surprisingly, one finds that the numerical results do not correspond to any *single*

TABLE III. Quasidegenerate GSs classified according to the IRREP of the $C_{6v} \otimes \mathcal{T}$ space group of the [1,1,1] topological sector of the 108 cluster.

IRREP	No. of $\mathbf{K}$	No. of states	No. of levels	GS energy levels	Total degen.[a]
$\Gamma(1,+,-)$	1	79 548 096	2	−3.657 214 41 −3.649 849 41	2
$\Gamma(1,+,+)$	1	79 548 096	2	−3.653 462 67 −3.646 352 04	2
$A(\times,+,-)$	3	238 642 176	2	−3.657 214 51 −3.649 849 60	6
$A(\times,+,+)$	3	238 642 176	2	−3.653 462 48 −3.646 351 92	6
$B(1,\times,-)$	2	159 073 536	2	−3.657 213 37 −3.649 849 46	4
$B(1,\times,+)$	2	159 073 536	2	−3.653 462 55 −3.646 352 03	4
$C(\times,\times,-)$	6	477 218 560	2	−3.657 213 33 −3.649 849 58	12
$C(\times,\times,+)$	6	477 218 560	2	−3.653 462 56 −3.646 351 92	12

[a]An extra (exact) degeneracy of 2 is expected for each level (see text).

VBC. However, they correspond exactly to the *reunion* of the GS multiplets of CVBC and VBC*.

VI. DISCUSSIONS

Our results clearly show a close competition between two (or even three) types of VBCs. We have checked that very small changes of the Hamiltonian parameters can easily reverse the relative position of the two subgroups of levels. Therefore it is not clear which of these VBC will be stabilized in the thermodynamic limit.

Let us first discuss the remarkable fine structure of the GS manifold in the [1,1,1] topological sector. It reflects the hidden Ising variable[17] associated to the two possible chiralities, say ↑ and ↓, of each of the resonating stars (or pinwheels) of the HVBC. On our 108-site cluster three

TABLE IV. Quasidegenerate GS classified according to the IRREP of the $C_{2v} \otimes \mathcal{T}$ space group of the [0,0,1] topological sector of the 108 cluster.

IRREP	No. of $\mathbf{K}$	No. of states	No. of levels	GS energy levels	Total degen.
$\Gamma^*(\times,+,+)$	1	238 613 056	2	−3.639 546 99 −3.639 460 27	2
$\Gamma^*(\times,+,-)$	1	238 613 056	2	−3.639 546 42 −3.639 458 83	2
$\Gamma^*(\times,-,+)$	1	238 613 056	1	−3.639 497 82	1
$\Gamma^*(\times,-,-)$	1	238 613 056	1	−3.639 495 81	1
$A_1(\times,+,+)$	1	238 605 760	1	−3.639 509 03	1
$A_1(\times,+,-)$	1	238 605 760	1	−3.639 509 00	1
$A_2(\times,+,\times)$	2	477 218 816	3	−3.639 508 79 −3.639 508 60 −3.639 497 19	6
$A_2(\times,-,\times)$	2	477 218 816	1	−3.639 496 79	2

such resonating stars can be fitted leading to $2^3 = 8$ possible configurations. The numerical spectrum can be explained by assuming a (small) effective "magnetic" Ising field h, which naturally provides splitting by energies $-3h$, $-h$, h, and $3h$. Although this structure is relatively robust and does not require real "fine tuning" of the effective model, the fact that $J_{12} = 0$ is important. Indeed, when J_{12} is added by hand, the numerical results can be simply interpreted by assuming a (strong) linear dependance of the effective Ising field with J_{12}, $h = h_0 + A J_{12}$, and h changes sign for a tiny (positive) value of $J_{12} \sim 0.001$. Similarly, a small value of $J_{12} = \pm 0.01$ increases the splitting within the GS manifold by a factor ~ 5. The behavior in the thermodynamic limit (for $J_{12} = 0$) depends crucially on whether the effective h_0 is exactly zero or retains a very small but still finite value. In the latter (most probable) case, the absolute HVBC GS should exhibit a uniform chirality of all resonating stars (one of the two ferromagnetic Ising configurations) and the VBC gap should be filled by a discrete set of energy levels corresponding to the excitations of a finite number of resonating stars. In contrast, in the unlikely case where $h_0 = 0$ (due to fine tuning) the HVBC GS would retain an infinite degeneracy.

Identifying the exact nature of the phase in the T_1, T_2, and T_3 topological sectors is more subtle. In fact, because of two (GS) energy levels in the fully symmetric $\Gamma^*(\times,+,+)$ IRREP this phase cannot be described as a unique VBC. From a direct comparison of the quantum numbers of the states in the GS manifold with those listed in Table II, our numerical data can indeed be interpreted as the simultaneous occurrence of two very closely competing VBCs, the columnar CVBC and the 2×2 VBC*. Such a description, however, raises a number of concerns. First, the exact nature of VBC* is not fully known: it is similar to SVBC in terms of symmetry properties but belongs to a different topological sector. A naive representation in terms of a simple NN dimer covering is therefore impossible and should involve subtle resonances like rVBC1 or rVBC2. Second, we have checked that the almost exact degeneracy between CVBC and VBC* is robust and survives under small changes of the QDM Hamiltonian parameters so that it does not correspond to any fine tunning. This unconventional feature might have different origins: (i) CVBC and VBC* are truly different but are related by some hidden symmetry of the original projected Heisenberg model or of its approximate effective model (1). (ii) The relevant phase still corresponds to a unique VBC of smaller degeneracy ($3 \times 8 = 24$ instead of $3 \times 16 = 48$) but admits some form of zero-energy excitations. It is interesting to note that Eq. (1) only contains loops of different lengths but always involving a *single* hexagon. It might be that smaller terms involving longer loops (and hence at least two hexagons) could lift this degeneracy. (iii) The observed degeneracy is the signature of an ordered phase which is more complex than a VBC. We could think, for instance, of some unconventional VBC with broken time-reversal symmetry. Although it is not clear to us how to construct precisely such a state, it may have $n_\Gamma = 2$. The tight competition between several VBCs in addition to the existence of a $\mathbb{Z}_2$ dimer liquid stable very nearby in parameter space[25] are clear signatures of the highly frustrated nature of the generalized QDM model, probably also generic in

several highly frustrated QHAFs. In fact, the observation in recent DMRG studies of the kagome QHAF[10] of signals of the formation of crystalline diamond patterns together with fingerprints of a $\mathbb{Z}_2$ *spin* liquid suggests that the QHAF and the effective QDM might have strong similarities. In any case, our results reveal an exceptionally large degeneracy of the GS multiplet ($96 + 48 = 144$ on our 108-site cluster!) in *all topological sectors*. If the same were to exist in a frustrated QHAF, we believe the related LED and DMRG results might become quite difficult to analyze. Incidentally, our study also shows that the existence of quasidegenerate GSs in *different* topological sectors (on the cylinder or on the torus) is not sufficient to characterize a $\mathbb{Z}_2$ dimer (or spin) liquid, our result

providing a counterexample. However, it might be a signature of the *close proximity* of the $\mathbb{Z}_2$ liquid in some enlarged parameter space.[25]

[1] M. Shores, E. Nytko, B. Bartlett, and D. Nocera, J. Am. Chem. Soc. **127**, 13462 (2005).

[2] A. Zorko, S. Nellutla, J. van Tol L. C. Brunel, F. Bert, F. Duc, J. C. Trombe, M. A. de Vries, A. Harrison, and P. Mendels, Phys. Rev. Lett. **101**, 026405 (2008).

[3] A. Olariu, P. Mendels, F. Bert, F. Duc, J. C. Trombe, M. A. de Vries, and A. Harrison, Phys. Rev. Lett. **100**, 087202 (2008).

[4] P. Mendels, F. Bert M. A. de Vries, A. Olariu, A. Harrison, F. Duc, J. C. Trombe, J. Lord, A. Amato, and C. Baines, Phys. Rev. Lett. **98**, 077204 (2007).

[5] P. Mendels and F. Bert, J. Phys. Soc. Jpn. **79**, 011001 (2010); see also P. Mendels and F. Bert, e-print arXiv:1107.3038, to be published in Journal of Physics: Conference Series.

[6] For a review, see P. Sindzingre, C. Lhuillier, and J.-B. Fouet, in *Recent Progress in Many-Body Theories*, edited by R. F. Bishop, T. Brandes, K. A. Gernoth, N. R. Walet, and Y. Xian, *Advances in Quantum Many-Body Theory* (World Scientific, Singapore, 2002), Vol. 6, p. 90; Int. J. Mod. Phys. B **17**, 5031 (2003).

[7] M. Hermele, Y. Ran, P. A. Lee, and X.-G. Wen, Phys. Rev. B **77**, 224413 (2008).

[8] P. W. Leung and Veit Elser, Phys. Rev. B **47**, 5459 (1993).

[9] H. C. Jiang, Z. Y. Weng, and D. N. Sheng, Phys. Rev. Lett. **101**, 117203 (2008).

[10] S. Yan, D. A. Huse, and S. R. White, Science **332**, 1173 (2011).

[11] Y. Iqbal, F. Becca, and D. Poilblanc, Phys. Rev. B **84**, 020407(R) (2011).

[12] Yuan-Ming Lu, Ying Ran, and Patrick A. Lee, Phys. Rev. B **83**, 224413 (2011).

[13] A. V. Syromyatnikov and S. V. Maleyev, Phys. Rev. B **66**, 132408 (2002).

[14] J. B. Marston and C. Zeng, J. Appl. Phys. **69**, 5962 (1991); SU(N) VBCs have been introduced by N. Read and S. Sachdev, Phys. Rev. B **42**, 4568 (1990).

[15] Ran Budnik and Assa Auerbach, Phys. Rev. Lett. **93**, 187205 (2004).

[16] P. Nikolic and T. Senthil, Phys. Rev. B **68**, 214415 (2003).

[17] R. R. P. Singh and D. A. Huse, Phys. Rev. B **76**, 180407 (2007).

[18] Y. Iqbal, F. Becca, and D. Poilblanc, Phys. Rev. B **83**, 100404(R) (2011); see also Ookie Ma and J. B. Marston, Phys. Rev. Lett. **101**, 027204 (2008).

[19] The relevance of the NNVB basis for the kagome QHAF has been investigated in M. Mambrini and F. Mila, Eur. Phys. J. B **17**, 651 (2000). Although the detailed dynamics of the valence bonds might be different in the effective QDM and in the original Heisenberg (spin) model, the effective QDM incorporates the presence of low-energy singlet states and competing resonance loops of different sizes, and correctly describes the *projected* spin model.

[20] D. S. Rokhsar and S. A. Kivelson, Phys. Rev. Lett. **61**, 2376 (1988).

[21] A. Ralko, M. Mambrini, and D. Poilblanc, Phys. Rev. B **80**, 184427 (2009).

[22] D. Schwandt, M. Mambrini, and D. Poilblanc, Phys. Rev. B **81**, 214413 (2010); Note crucial differences with previous work, C. Zeng and V. Elser, *ibid.* **51**, 8318 (1995).

[23] G. Misguich, D. Serban, and V. Pasquier, Phys. Rev. Lett. **89**, 137202 (2002).

[24] R. Moessner and S. L. Sondhi, Phys. Rev. Lett. **86**, 1881 (2001).

[25] D. Poilblanc, M. Mambrini, and D. Schwandt, Phys. Rev. B **81**, 180402 (2010).

[26] A. Ralko, F. Becca, and D. Poilblanc, Phys. Rev. Lett. **101**, 117204 (2008).

[27] D. Poilblanc and A. Ralko, Phys. Rev. B **82**, 174424 (2010).

[28] C. Xu and S. Sachdev, Phys. Rev. B **79**, 064405 (2009); Yejin Huh, Matthias Punk, and Subir Sachdev, *ibid.* **84**, 094419 (2011).

[29] G. Misguich and P. Sindzingre, J. Phys.: Condens. Matter **19**, 145202 (2007) (note that the more recent unpublished e-print arXiv:cond-mat/0607764v3 includes small corrections).

[30] Note that the Lanczos algorithm can provide the level degeneracies by applying successive runs starting from different initial conditions and then by computing the rank of the overlap matrix of the set of (possibly different) generated GSs.